# Optimal Loop Shaping and Disturbance Rejection Beyond the Nyquist Frequency using a Forward Model Disturbance Observer and Convex Optimization Based Filter Design

Thomas L. Chu†, Xiaohai Hu†, and Xu Chen†,⋆

***Abstract*— Loop shaping based on the disturbance observer (DOB) offers great flexibility in designing a control system's closed-loop sensitivity to external disturbances and noises. While it is well understood how to design feedback control to reject band-limited disturbances with little trade-off when a closed-loop system has a single sampling control rate, challenges arise when disturbances appear beyond the Nyquist frequency and when the speed of the feedback sensor cannot be conveniently increased due to hardware and/or process constraints. Such is the case in hard disk drives and emerging vision-based motion control. In this paper, we propose an optimal multirate forward model disturbance observer (MFMDOB) for intuitive, flexible, and exact rejection of band-limited disturbances beyond the Nyquist frequency. Based on the tools from Youla-Kucera parameterization, the internal model principle, multirate analysis, and convex optimization, we translate the design objective into a set of model-based convex optimization and multirate prediction problems, enabling optimal local-loop shaping (LLS). We provide different optimal design formulations with finite and infinite impulse response filters. Verification of the MFMDOB is conducted on a galvo scanning process model in selective laser sintering for additive manufacturing.**

## I. Introduction

An essential task in precision motion control is to shape the feedback loop locally to reject band-limited disturbances. This practice, known as local-loop shaping (LLS), is fundamental for ensuring nanometer precision in applications like hard disk drives (HDDs) and semiconductor manufacturing [1], [2]. LLS primarily involves creating notch shapes in the closed-loop error-rejection function, a process that must adhere to the inherent constraints of feedback control design. In particular, the disturbance observer (DOB) employs model inversion for intuitive LLS and has proven effective in precision information storage and manufacturing [3], [4]. The concept also extends to systems with unstable inverses, leading to the development of the forward model selective disturbance observer (FMSDOB) that avoids explicit model inversion [5].

When the feedback sampling rate lags behind the core system dynamics, traditional LLS encounters inherent bandwidth constraints. For example, in visual servoing where the sensor's data-intensive nature limits its sampling rate, robot manipulators are susceptible to latency and bandwidth restrictions [6]. Similarly, when processes like selective laser sintering (SLS) adopt visual feedback (e.g. infrared vision), the sensor operates at a significantly slower rate compared to the speed of the material processing [7]. In these scenarios, disturbances occurring beyond the Nyquist frequency of the slow feedback sensor are not fully observable due to downsampling and aliasing.

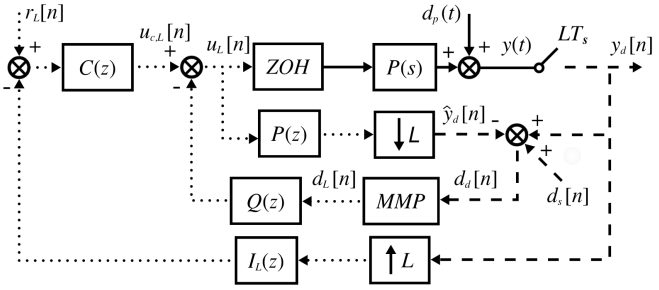


Fig. 1. Block diagram of the proposed MFMDOB. The sampling times are indicated by the dashed (slower, $LT_s$) and the dotted (faster, $T_s$) lines. The continuous-time signals are indexed by $(\cdot)$, and discrete-time signals by $[\cdot]$ (e.g. $r(t)$ is a continuous-time signal, and $r[n]$ is a discrete-time signal).

To overcome the limitations posed by slow feedback sensors, this paper proposes an optimal multirate forward model disturbance observer (MFMDOB) which is capable of reconstructing structured disturbances that occur beyond the Nyquist frequency. We leverage the internal model principle and Youla-Kucera all-stabilizing control to assure high-performance disturbance rejection while assuring closed-loop stability beyond the Nyquist frequency. To cope with the aliasing effect, optimality is then introduced to ensure disturbance rejection at the target frequencies while simultaneously minimizing error amplification across other frequencies, both below and above the Nyquist frequency. Our approach incorporates various design options using both finite and infinite impulse response filters. The coefficients for these filters were obtained by forming a set of convex optimization problems involving second-order conic programming (SOCP) and semi-definite programming (SDP).

## II. Control Design

### A. Problem Formulation

Fig. 1 shows the block diagram of the proposed MFMDOB. We focus on the case where the system is single-input single-output (SISO). The proposed MFMDOB uses the principles from internal model control, where the forward model is leveraged and the inverse dynamics of the plant

† T. L. Chu (email: tchu@uw.edu), X. Hu (email: huxh@uw.edu), and X. Chen (email: chx@uw.edu) are with the Mechanical Engineering Department, University of Washington, Seattle, WA 98195. ⋆: corresponding author.

is then parameterized through a performance-enhancement filter $Q(z)$. When all signals have the same sampling rate, the inner-loop structure is in fact a form of Youla-Kucera all-stabilizing control [8]. Here, $P(s)$ and $P(z)$ are the continuous- and fast-sampled discrete-time plant models. $y(t)$ is the immediate continuous-time plant output, and $y_d[n]$ is the actual measurable slow sampled output. A discrete-time estimate of the disturbance $d_p(t)$ is formed in $d_d[n]$, which is upsampled and refined in the mulirate model predictor (MMP) and $Q(z)$. As a result of this sequence of filtering, the output of $Q(z)$ serves to counteract the effect of the disturbance $d_p(t)$ at a rate beyond the Nyquist frequency of the original output sampler $LT_s$. In this implementation, the control structure does not require model inversion and applies to stable *minimum-* or *non-minimum phase* (NMP) plants.

Other than the aforementioned notations and signal flows, $y_d[n]$ is upsampled from the slow sampling time, $LT_s$, in the baseline control, to the fast sampling time, $T_s$, by a factor of $L$ to match the controller input sampling time. The upsampled signal passes through an interpolator, $I_L(z)$, with a zero order hold (ZOH) operating at the speed of $T_s$. $r_L[n]$ is the reference input. $u_{c,L}[n]$ and $u_L[n]$ are the baseline control output and the final plant input. Also, $\hat{y}_d[n]$ is the estimated disturbance-free output sampled at the same speed as $y_d[n]$; $d_s[n]$ is the sensor noise; $d_d[n]$ and $d_L[n]$ are the estimated disturbances sampled at $LT_s$ and $T_s$, respectively. $\boxed{\uparrow L}$ and $\boxed{\downarrow L}$ are upsampling and downsampling operations, respectively.

A structured disturbance can be modeled as the output of a system excited by an impulse signal $\delta[n]$ [9]. For instance, a constant $d[k] = d$ is the impulse response of the scaled integrator $d/(1-z^{-1})$; $\sin(\omega_0 k)$ is the impulse response of the filter $(z^{-1}\sin\omega_0)/(1-2z^{-1}\cos\omega_0+z^{-2})$. More generally, we model the disturbance as $d[k] = B_d(z^{-1})/A_d(z^{-1})\delta[k]$ in the z-domain [7], [10], where $z^{-i}$ for $i > 0$ denotes the backward shift operator [11]. When we rewrite such a relationship as $A_d(z^{-1})d_L[n] = B_d(z^{-1})\delta[n]$, the right-hand side is a linear combination of delayed and scaled impulses that converge to zero, which implies that $A_d(z^{-1})d_L[n] \to 0$. Perfect multirate disturbance rejection is then feasible by constructing a set of Diophantine equations that are analytically solvable to recover the structured disturbance at integer fractions of the slow sensor sampling rate [12].

For completeness, we review the key results in the disturbance reconstruction, and then in the next subsection, we focus on the key results of convex-optimization based LLS. We focus on the band-limited disturbance $d_p(t) = \eta(t)+\sum_{i=1}^{m}\lambda_{d,i}\sin(2\pi f_{d,i}t+\phi_{d,i})$, where $\lambda_{d,i}$ and $\phi_{d,i}$ are an unknown amplitude and phase shift of the narrow-band disturbance component, and $\eta(t)$ characterizes other broad-band noises. The disturbance frequency, $f_{d,i}$ (Hz), can be acquired through spectrum analysis and system identification and is assumed to be known or can be adaptively estimated [13], [14]. When $m$ narrow-band disturbances are sampled at a sampling time of $T_s$, the disturbance-model polynomial $A_d(z^{-1})$ is

$$\begin{aligned} A_d(z^{-1}) &= \prod_{i=1}^{m}\left(1-2\cos(2\pi f_{d,i}T_s)z^{-1}+z^{-2}\right) \\ &= 1+a_1z^{-1}+\ldots+a_{2m}z^{-2m} \end{aligned} \tag{1}$$

We design the fast-sampling to divide the slow-sampling time, such that $d_d[n] = d_p(nT_sL)$ and $d_d[n] = d_L[nL]$. There are $L-1$ intersample points between $d_d[n]$ and $d_d[n+1]$ required to rebuild the lost signal. Let $k \in \{1,\ldots,L-1\}$ be the $k^{\text{th}}$ intersample point between $d_L[nL]$ and $d_L[(n+1)L]$. We construct the Diophantine equation

$$F_k(z^{-1})A_d(z^{-1}) + z^{-k}W_k(z^{-L}) = 1 \tag{2}$$

with

$$F_k(z^{-1}) = 1+f_{k,1}z^{-1}+\ldots+f_{k,2m(L-1)}z^{-2m(L-1)} \tag{3}$$

$$W_k(z^{-L}) = w_{k,0}+w_{k,1}z^{-L}+\ldots+w_{k,n_w}z^{-(n_w)L} \tag{4}$$

where $n_w \geq 2m-1$. The minimum-order solution ($n_w = 2m-1$) to Eq. (2) is solved by matching the coefficients of Eqs. (3) and (4) with respect to $z^{-i}$, which is expressed as the linear matrix equation

$$M_k\begin{bmatrix} f_{k,1} \\ \vdots \\ f_{k,2m(L-1)} \\ w_{k,0} \\ \vdots \\ w_{k,n_w} \end{bmatrix} = \begin{bmatrix} -a_1 \\ -a_2 \\ \vdots \\ -a_{2m} \\ 0 \\ \vdots \\ 0 \end{bmatrix} \tag{5}$$

where $M_k \in \mathbb{R}^{2mL\times 2mL}$ is defined as

$$M_k = \begin{bmatrix} \tilde{M}_k & | & e_k & e_{k+L} & \cdots & e_{k+(2m-1)L} \end{bmatrix} \tag{6}$$

and $e_i$ is a column vector of zeros except for the $i^{\text{th}}$ row, which is one. $\tilde{M}_k$ is defined as

$$\tilde{M}_k = \begin{bmatrix} 1 & \cdots & 0 \\ \vdots & \ddots & \vdots \\ a_{2m} & \ddots & 1 \\ \vdots & \ddots & \vdots \\ 0 & \cdots & a_{2m} \end{bmatrix}_{2mL\times 2m(L-1)} \tag{7}$$

Multiplying Eq. (2) by $d_L[n]$ and applying the internal signal model of $A_d(z^{-1})d_L[n] \to 0$, we have, at steady state

$$d_L[n] = W_k(z^{-L})d_L[n-k] \tag{8}$$

Substituting Eq. (4) into Eq. (8) and letting $n = nL+k$ yield $d_L[nL+k] = \sum_{i=0}^{2m-1} w_{k,i}d_L[(n-i)L]$, or equivalently, after using the notation in the multirate block diagram,

$$d_L[nL+k] = \sum_{i=0}^{n_w} w_{k,i}d_d[n-i] \tag{9}$$

Thus, the disturbance signal is reconstructed at the fast sampling frequency. $1/T_s$.

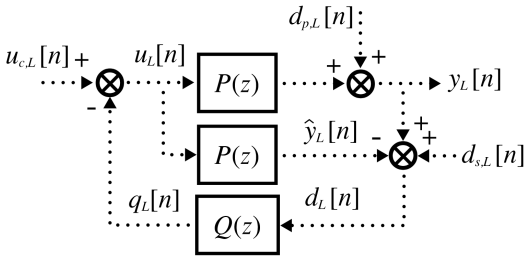


Fig. 2. Forward model DOB loop.

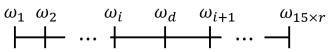


Fig. 3. A set of discrete frequencies with one disturbance frequency where $0 < \omega_1 < \omega_2 < \ldots < \omega_{15\times r} \leq \pi$ (rad).

### *B. Convex-Optimization Based Optimal Local-Loop Shaping*

We now discuss the main optimal LLS design. In this subsection, let us assume that the feedback sampling time in Fig. 1 is fast ($L = 1$). As $P(z)$ is the ZOH equivalent of $P(s)$ sampled at $T_s$, the output satisfies $y_L[n] = y(nT_s)$. When no modeling error exists, $\hat{y}_L[n]$ is disturbance free. We then have $d_{p,L}[n] = y_L[n] - \hat{y}_L[n]$. Fig. 2 shows the output of the system in the z-domain, where the transfer function from the plant disturbance to the output is

$$\frac{Y_L}{D_{p,L}}(z) = 1 - P(z)Q(z) \tag{10}$$

For effective disturbance rejection while permitting non-disturbance signals to pass, the ideal conditions for Eq. (10) are

$$1 - P(e^{j\omega_{d,i}})Q(e^{j\omega_{d,i}}) = 0 \tag{11}$$

$$P(e^{j\omega_i})Q(e^{j\omega_i}) = 0 \tag{12}$$

where $\omega_{d,i}$ (rad) denotes the $i^{\text{th}}$ disturbance frequency, and $\omega_i$ (rad) belongs to the set of uniformly distributed non-disturbance frequencies. The constraints of the parameterized finite impulse response (FIR) filter in continuous-time is accurately approximated in the discrete-time as a set of $15 \times r$ uniformly spaced discrete frequencies spanning from 0 to $\pi$ rad, where $r$ is the filter order [15]. To avoid infeasibility between the band-stop (BS) and band-pass (BP) constraints of Eqs. (11) and (12), respectively, the closest non-disturbance frequencies below and above each disturbance frequency is spaced such that $\omega_i = \omega_d - \pi/(2 \times r)$ and $\omega_{i+1} = \omega_d + \pi/(2 \times r)$. Fig. 3 illustrates an example set of discrete frequencies.

*1) Convex Optimization of Q(z) using Second-Order Conic Programming:* In this subsection, we formulate Eq. (12) into a quadratic constraint for SOCP that is solved using the interior point method [16]. Let the plant and filter design of be described as

$$P(z) = \frac{b_{m_p} z^{m_p} + \ldots + b_1 z + b_0}{z^{n_p} + a_{n_p-1} z^{n_p-1} + \ldots + a_1 z + a_0} \tag{13}$$

$$Q(z) = q_0 + q_1 z^{-1} + \cdots + q_r z^{-r} \tag{14}$$

where $n_p > m_p \geq 0$ and $\{q_0 \ldots q_r\}$ are the FIR filter coefficients. The equalities of Eqs. (11) and (12) are linear for every $\omega_{d,i}$ and $\omega_i$. More specifically, let us express Eq. (14) as a dot product

$$Q(z) = q^T \phi(z) \tag{15}$$

where $q = \begin{bmatrix} q_0 & q_1 & \cdots & q_r \end{bmatrix}^T$ and $\phi(z) = \begin{bmatrix} 1 & z^{-1} & \cdots & z^{-r} \end{bmatrix}^T$. Substituting $z = e^{j\omega_i}$, Eq. (15) is divided into real and imaginary components such that

$$Q(e^{j\omega_i}) = q^T \phi_r(e^{j\omega_i}) - j q^T \phi_i(e^{j\omega_i}) \tag{16}$$

where $\phi_r(e^{j\omega_i}) = \begin{bmatrix} 1 & \cos(\omega_i) & \cdots & \cos(r\omega_i) \end{bmatrix}^T$ and $\phi_i(e^{j\omega_i}) = \begin{bmatrix} 0 & \sin(\omega_i) & \cdots & \sin(r\omega_i) \end{bmatrix}^T$. Let the plant at $z = e^{j\omega_i}$ be divided into real and imaginary components, where $P = P_r + jP_i$ (the term, $e^{j\omega_i}$, is omitted here and forward for brevity). Substituting Eq. (16) into Eq. (11) yields

$$q^T \left(P_r \phi_r - P_i \phi_i\right) - j q^T \left(P_i \phi_r + P_r \phi_i\right) q = 1 \tag{17}$$

Eq. (17) is a linear equality with respect to $q$ and therefore convex; thus, Eq. (11) is convex.

Eq. (12) is not practical, so the constraint is relaxed to an upper bound where $|P(e^{j\omega_i})Q(e^{j\omega_i})| \leq \beta(\omega_i)$. Taking the square yields

$$q^T \left[\phi_r (P_r^2 + P_i^2) \phi_r^T + \phi_i (P_r^2 + P_i^2) \phi_i^T\right] q \leq \rho(\omega_i) \tag{18}$$

Thus, Eq. (18) is a quadratic inequality; the number of inequalities, denoted as $n_m$, is dependent on the set of discrete non-disturbance frequency range to be minimized.

Integrating both the BS and BP signal criteria, the proposed SOCP for optimal LLS is

$$\begin{aligned} \min_{\rho} \quad & \sum_{i=1}^{n_m} \rho(\omega_i) \\ \text{subject to} \quad & 1 - P(e^{j\omega_{d,i}})Q(e^{j\omega_{d,i}}) = 0 \qquad \forall i = 1, \ldots, m \\ & q^T [\phi_r (P_r^2 + P_i^2) \phi_r^T \ldots \\ & + \phi_i (P_r^2 + P_i^2) \phi_i^T] q \leq \rho(\omega_i) \quad \forall i = 1, \ldots, n_m \end{aligned} \tag{19}$$

This formulation has several advantages. First, the relaxed constraint from Eq. (18) allows solvers to automatically determine a feasible solution. Second, the minimum bound $\rho(\omega_i)$ is automatically solved from optimization, and the designer possesses the discretion to select the frequency range for minimization.

*2) Finite Impulse Response Filter Formulation using Semi-Definite Programming:* We have applied SOCP for solving a feasible bound for the BP constraint in Eq. (18). However, the SOCP does not directly minimize amplifications in Eq. (10) rooted in the celebrated Bode's Integral Theorem. To address this, we formulate the objective function to minimize the $H_\infty$ norm (maximum magnitude response) of Eq. (10), using a special form of the discrete-time Bounded-Real lemma.

*Discrete-Time Bounded-Real Lemma.* Let $G(z)$ denote a discrete-time system that is LTI with a minimal state-space

realization. The inequality $\|G(z)\|_\infty \leq \gamma$ is satisfied if $G(z)$ is bounded-input, bounded-output (BIBO) stable [17], and there exists a positive semi-definite matrix $M$ such that the following matrix inequality holds [18], [19]

$$\begin{bmatrix} M & MA_d & MB_d & \mathbf{0} \\ A_d^T M & M & \mathbf{0} & C_d^T \\ B_d^T M & \mathbf{0} & \gamma \mathbf{I} & D_d^T \\ \mathbf{0} & C_d & D_d & \gamma \mathbf{I} \end{bmatrix} \preceq 0 \tag{20}$$

In the proposed solution, we transform $G(z)$ from Eq. (10) into its controllable canonical form (CCF), which stores the coefficients of $Q(z)$, $q$ (in vector form), in matrices $C_d$ and $D_d$. As a result, the matrix inequality in Eq. (20) becomes linear in terms of both $q$ and $M$, preserving convexity. Other state-space representations of the Bounded-Real Lemma (see, e.g., [20]) can be used, but linearity with respect to $q$ and $M$ must be preserved in the matrix inequality.

Given the discrete-time system represented by Eq. (13), the state-space representation in the CCF is

$$x_P[n+1] = A_P x_P[n] + B_P u[n] \tag{21}$$
$$y_P[n] = C_P x_P[n] + D_P u[n] \tag{22}$$

with

$$A_P = \begin{bmatrix} 0 & 1 & \cdots & 0 \\ \vdots & \vdots & \ddots & \vdots \\ 0 & 0 & \cdots & 1 \\ -a_0 & -a_1 & \cdots & -a_{n_P-1} \end{bmatrix} \quad B_P = \begin{bmatrix} 0 \\ \vdots \\ 0 \\ 1 \end{bmatrix}$$
$$C_P = \begin{bmatrix} b_0 & \cdots & b_{m_p} & \mathbf{0^{1x(n_p-m_p-1)}} \end{bmatrix} \quad D_P = [0] \tag{23}$$

Note that the input for $Q(z)$ is the output of $P(z)$. The state-space representation of Eq. (14) in CCF is

$$x_Q[n+1] = A_Q x_Q[n] + B_Q y_P[n] \tag{24}$$
$$y_Q[n] = C_Q x_Q[n] + D_Q y_P[n] \tag{25}$$

with

$$A_Q = \begin{bmatrix} 0 & 1 & \cdots & 0 \\ \vdots & \vdots & \ddots & \vdots \\ 0 & 0 & \cdots & 1 \\ 0 & 0 & \cdots & 0 \end{bmatrix} \quad B_Q = \begin{bmatrix} 0 \\ \vdots \\ 0 \\ 1 \end{bmatrix}$$
$$C_Q = \begin{bmatrix} q_r & q_{r-1} & \cdots & q_1 \end{bmatrix} \quad D_Q = [q_0] \tag{26}$$

Let the state variable be $\tilde{x}[n] = \begin{bmatrix} x_P^T[n] & x_Q^T[n] \end{bmatrix}^T$. The state-space representation of Eq. (10) is

$$\tilde{x}[n+1] = \tilde{A}\tilde{x}[n] + \tilde{B}u[n] \tag{27}$$
$$\tilde{y}[n] = \tilde{C}\tilde{n}[n] + \tilde{D}u[n] \tag{28}$$

with

$$\tilde{A} = \begin{bmatrix} A_P & \mathbf{0_{n_p \times r}} \\ B_Q C_P & A_Q \end{bmatrix} \quad \tilde{B} = \begin{bmatrix} B_P \\ B_Q D_P \end{bmatrix}$$
$$\tilde{C} = -\begin{bmatrix} D_Q C_P & C_Q \end{bmatrix} \quad \tilde{D} = [1 - D_Q D_P] \tag{29}$$

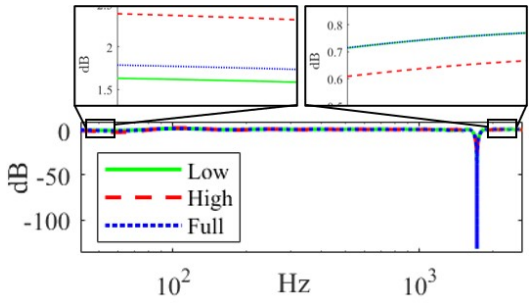


Fig. 4. Bode plot of Eq. (10) using SOCP of Eq. (19). The solid green line, denoted as "Low", represents the minimization below the disturbance frequency of 1716 Hz. The dashed red line, denoted as "High", represents the minimization above 1716 Hz. The dotted blue line, denoted as "Full", represents the minimization spanning the entire frequency range.

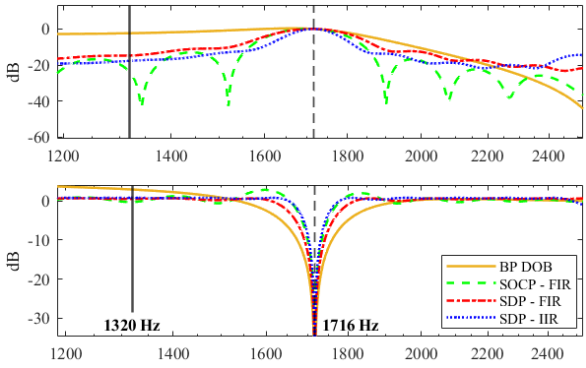


Fig. 5. Bode plots of $P(z)Q(z)$ (top) and Eq. (10) (bottom). The Nyquist frequency is 1320 Hz, and the disturbance frequency is 1716 Hz.

Applying Eq. (20) to the state-space from Eq. (29), we have the minimization problem for the SDP-FIR filter

$$\begin{aligned} &\min_{\gamma, M} \quad \gamma \\ &\text{subject to} \quad 1 - P(e^{j\omega_{d,i}})Q(e^{j\omega_{d,i}}) = 0 \qquad \forall i = 1, \ldots, m \\ &\begin{bmatrix} M & M\tilde{A} & M\tilde{B} & \mathbf{0} \\ \tilde{A}^T M & M & \mathbf{0} & \tilde{C}^T \\ \tilde{B}^T M & \mathbf{0} & \gamma \mathbf{I} & \tilde{D}^T \\ \mathbf{0} & \tilde{C} & \tilde{D} & \gamma \mathbf{I} \end{bmatrix} \preceq 0 \\ &M \succeq 0, \ \gamma \geq 0 \\ &q^T[\phi_r(P_r^2 + P_i^2)\phi_r^T + \ldots \\ &\quad \phi_i(P_r^2 + P_i^2)\phi_i^T]q \leq \rho(\omega_i) \qquad \forall i = 1, \ldots, n_m \end{aligned} \tag{30}$$

*3) Infinite Impulse Response Filter Formulation using Semi-Deifnite Programming:* In addition to the FIR filter design, infinite impulse response (IIR) filters provide a versatile design approach for LLS. We provide an optimal IIR notch filter design to match the performance of the SDP-FIR filter at a reduced filter order. Specifically, the proposed IIR filter has the form

$$Q_{IIR}(z) = (1 - V(z))\, K(z) \tag{31}$$

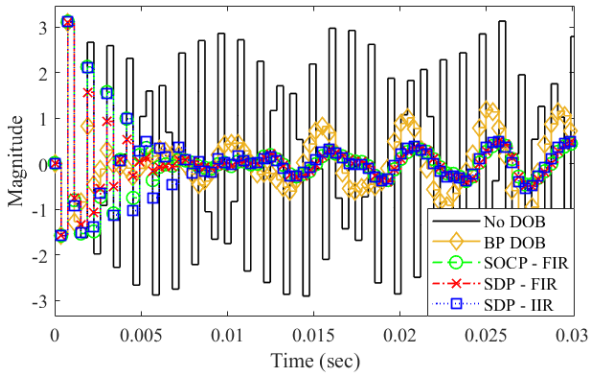


Fig. 6. Measured slow output (sampled at $T_s$) of the system without the DOB, baseline BP FMSDOB, FIR filters, and IIR filter.

with

$$V(z) = \prod_{i=1}^{m} \frac{1 - 2z^{-1}\cos\omega_{d,i} + z^{-2}}{1 - 2\alpha_i z^{-1}\cos\omega_{d,i} + \alpha_i^2 z^{-2}} \tag{32}$$

$$K(z) = k_0 + k_1 z^{-1} + \cdots + k_r z^{-r} \tag{33}$$

where $\alpha_i \in (0, 1)$ controls the notch size. As $\alpha$ approaches zero, the disturbance rejection notch width expands. The minimization for the IIR filter is similar to the SDP-FIR filter. Let $P = N_p(z)/D_p(z)$ and $V = N_v(z)/D_v(z)$. Substituting Eq. (31) into Eq. (10) yields

$$1 - P(z)Q_{IIR}(z) = 1 + H(z)K(z) \tag{34}$$

with

$$H(z) = \frac{N_p(z)N_v(z) - N_p(z)D_v(z)}{D_p(z)D_v(z)} \tag{35}$$

The state-space formulations of $H(z)$ and $K(z)$ are similar to Eqs. (23) and (26) and are omitted for brevity. Let the state variable for Eq. (34) be $\bar{x}[n] = \begin{bmatrix} x_H^T[n] & x_K^T[n] \end{bmatrix}^T$, where $x_H[n]$ and $x_K[n]$ are the state variables for $H(z)$ and $K(z)$ respectively. The state-space representation of Eq. (34) in CCF is

$$\begin{aligned} \bar{x}[n+1] &= \bar{A}\bar{x}[n] + \bar{B}u[n] \\ \bar{y}[n] &= \bar{C}\bar{x}[n] + \bar{D}u[n] \end{aligned} \tag{36}$$

with

$$\begin{aligned} \bar{A} &= \begin{bmatrix} A_H & \mathbf{0}_{n_h \times r} \\ B_K C_H & A_K \end{bmatrix} & \bar{B} &= \begin{bmatrix} B_H \\ B_K D_H \end{bmatrix} \\ \bar{C} &= \begin{bmatrix} D_K C_H & C_K \end{bmatrix} & D_P &= [1 + D_K D_H] \end{aligned} \tag{37}$$

The minimization problem for the SDP-IIR filter is identical to Eq. (30).

## III. Numerical Verification

Simulation was conducted with MATLAB Simulink using the block diagram in Fig. 1. Consider the following plant from laser beam steering in selective laser sintering in additive manufacturing [5] and a discrete-time PID controller

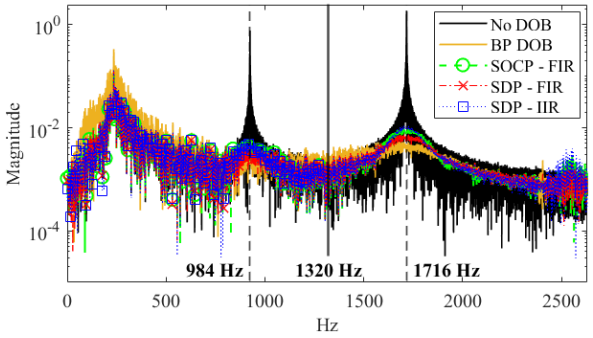


Fig. 7. Spectra of the measured output with various DOB designs. The slow feedback sensor aliases the disturbance frequency at 1716 Hz and appears at 984 Hz.

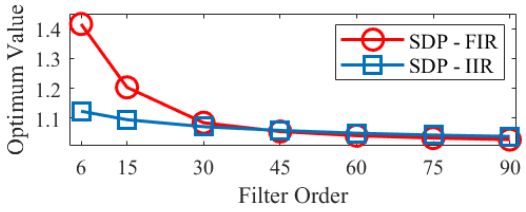


Fig. 8. Comparison of the optimal value of the SDP-FIR and SDP-IIR filters at various filter orders.

with a sampling time of $T_s = 1/5280$ second

$$P(s) = \frac{3.74488 \times 10^9}{s^2 + 565.5s + 3.197752 \times 10^5}$$

$$C(z) = \frac{1}{200}\left[0.125 + \frac{0.05}{z-1} + \frac{0.6(z-1)}{z}\right]$$

We focused on the slow sensor with half the sampling rate of the input ($L = 2$, $f_{ss} = 2/T_s = 2640$ Hz with the Nyquist frequency at 1320 Hz). The filter order was $r = 30$, and the disturbance frequency was $1.3 \times f_{ss}/2 = 1716$ Hz. The fast-rate disturbance signal was reconstructed using Eqs. (1) - (9). The disturbance amplitude was $\lambda = 2$ with a random phase shift $\phi \in [0, \pi]$. White Gaussian noise was introduced as the plant disturbance, $d_p(t)$, and sensor noise, $d_s[n]$, at unity power. The SOCP and SDP from Eqs. (19) and (30) were used to design $Q(z)$. The BP FMSDOB from [5] was used as the baseline DOB for comparison.

Fig. 4 shows the Bode plot of Eq. (10) using the SOCP FIR filter with various frequency ranges constrained in Eq. (19). In all solutions, there were large disturbance rejection at 1716 Hz, and the magnitudes of the "Low" and "High" lines were lowest below and above 1716 Hz, respectively. Notably, the magnitude of the "Full" line lies between the "Low" and "High" lines. Fig. 5 shows the bode plots of $P(z)Q(z)$ and Eq. (10), where the SOCP-FIR, SDP-FIR, and SDP-IIR filters outperformed the BP FMSDOB filter with low gains across the non-disturbance frequencies due to SDP and SOCP objective functions minimizing Eqs. (10) and (18), respectively.

The simulation output in Fig. 6 and the Fast Fourier Transform (FFT) of the output in Fig. 7 show that the optimally solved MFMDOBs minimized low frequency amplification

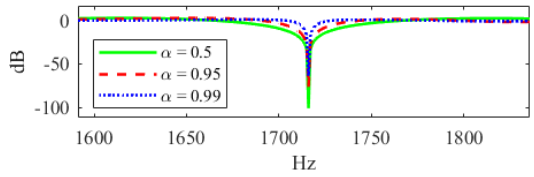


Fig. 9. Bode plot of (10) using the IIR filter at various $\alpha$'s.

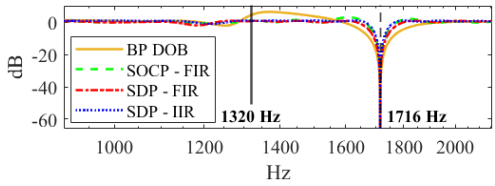


Fig. 10. Bode plot of (10) on a randomly generated 16th order system with a NMP zero.

compared to the BP FMSDOB. As the actual disturbance at 1716 Hz was beyond the Nyquist sampling frequency, the dual peaks observed at 984 Hz and 1716 Hz are symmetric about 1320 Hz, which indicates aliasing.

Fig. 8 shows the solved optimal value, $\gamma$, at various filter orders, indicating the maximum upper bound of $\|1 - P(z)Q(z)\|_\infty$. The lowest feasible filter order using SDP was six, and the IIR filter had a better optimum than the FIR filter up to a filter order of 30. There were diminishing returns increasing the filter order beyond 30. Fig. 9 shows the added benefit of adjusting the BS notch size for the IIR filter.

The robustness of the proposed algorithm was tested on randomly generated stable discrete-time plants with NMP zeros; the poles of the plant could have an integrator, repeated poles, and complex conjugate poles within the unit circle. The proposed algorithm found feasible solutions up to a plant order of $n_p = 16$. Table I shows the attenuation of the disturbance frequency and optimum values of the randomized discrete-time plants with NMP zeros. Fig. 10 shows an example of the Bode plot of the $16^{\text{th}}$ order plant with a NMP zero, where the proposed filters have less amplification below the disturbance frequency compared to the BP FMSDOB.

## IV. Conclusion

We proposed an optimally designed MFMDOB to attenuate structured disturbances beyond the Nyquist frequency of a feedback sensor. We presented the signal reconstruction process and posed the design prerequisites of the DOB into convex constraints for SOCP and SDP. Simulations were conducted to validate the efficacy of the MFMDOB employing SOCP-FIR, SDP-FIR, and SDP-IIR filters. The advantages of each optimally derived filter were discussed.

TABLE I

Simulation Results of $16^{\text{TH}}$ Order Discrete-Time Plants: Attenuation at 1716 Hz & Optimal Value

| Plant | SOCP FIR (Att.↓ / Opt.↓) | SDP FIR (Att.↓ / Opt.↓) | SDP IIR (Att.↓ / Opt.↓) |
|---|---|---|---|
| I (4 NMP zeros) | −162.4/8.212 | −165.6/1.178 | −169.3/1.112 |
| II (1 NMP zero) | −173.7/6.502 | −161.0/1.145 | −154.1/1.069 |
| III (2 NMP zeros) | −205.2/7.865 | −132.1/1.095 | −117.6/1.116 |

The optimal value for the SOCP FIR filter is $\sum \rho(\omega_i)$ from Eq. (19). The optimal value for the SDP filters is $\|1 - P(z)Q(z)\|_\infty$.

## References


[1] P. Weaver and R. Ehrlich, "The use of multirate notch filters in embedded-servo disk drives," in *Proceedings of 1995 American Control Conference - ACC'95*, vol. 6, 1995, pp. 4156–4160 vol.6.

[2] H. Fujimoto and Y. Hori, "Vibration suppression and optimal repetitive disturbance rejection control in semi-nyquist frequency region using multirate sampling control," in *Proceedings of the 39th IEEE Conference on Decision and Control*, vol. 4, 2000, pp. 3745–3750 vol.4.

[3] X. Chen and M. Tomizuka, "Overview and new results in disturbance observer based adaptive vibration rejection with application to advanced manufacturing," *International Journal of Adaptive Control and Signal Processing*, vol. 29, pp. 1459–1474, 2015.

[4] X. Chen, T. Jiang, and M. Tomizuka, "Pseudo youla–kucera parameterization with control of the waterbed effect for local loop shaping," *Automatica*, vol. 62, pp. 177–183, 2015.

[5] T. Jiang, H. Xiao, J. Tang, L. Sun, and X. Chen, "Local loop shaping for rejecting band-limited disturbances in nonminimum-phase systems with application to laser beam steering for additive manufacturing," *IEEE Transactions on Control Systems Technology*, vol. 28, no. 6, pp. 2249–2262, 2020.

[6] C. Wang, C.-Y. Lin, and M. Tomizuka, "Statistical learning algorithms to compensate slow visual feedback for industrial robots," *Journal of Dynamic Systems, Measurement, and Control*, vol. 137, no. 3, p. 031011, 10 2014.

[7] H. Xiao, T. Jiang, and X. Chen, "Rejecting fast narrow-band disturbances with slow sensor feedback for quality beam steering in selective laser sintering," *Mechatronics*, vol. 56, pp. 166–174, 2018.

[8] E. Hedberg, J. Löfberg, and A. Helmersson, "A pedagogical path from the internal model principle to youla-kučera parametrization," *IFAC-PapersOnLine*, vol. 53, no. 2, pp. 17 374–17 379, 2020, 21st IFAC World Congress.

[9] K. Ogata, *Discrete-Time Control Systems*, 2nd ed. Prentice-Hall, 1995.

[10] X. Chen and H. Xiao, "Multirate forward-model disturbance observer for feedback regulation beyond nyquist frequency," *Systems and Control Letters*, vol. 94, pp. 181–188, 2016.

[11] G. F. Franklin, J. D. Powell, and A. Emami-Naeini, *Feedback Control of Dynamic Systems*, 7th ed. Pearson, 2015.

[12] C. E. Garcia and M. Morari, "Internal model control. a unifying review and some new results," *Industrial & Engineering Chemistry Process Design and Development*, vol. 21, no. 2, pp. 308–323, 1982.

[13] X. Chen and M. Tomizuka, "A minimum parameter adaptive approach for rejecting multiple narrow-band disturbances with application to hard disk drives," *IEEE Transactions on Control Systems Technology*, vol. 20, no. 2, pp. 408–415, 03 2012.

[14] "Benchmark on adaptive regulation—rejection of unknown/time-varying multiple narrow band disturbances," *European Journal of Control*, vol. 19, no. 4, pp. 237–252, 2013.

[15] S.-P. Wu, S. Boyd, and L. Vandenberghe, "Fir filter design via semidefinite programming and spectral factorization," in *Proceedings of 35th IEEE Conference on Decision and Control*, vol. 1, 1996, pp. 271–276 vol.1.

[16] F. Alizadeh and D. Goldfarb, "Second-order cone programming," *Mathematical Programming*, vol. 95, pp. 3–51, 2003.

[17] S. Boyd, L. E. Ghaoui, and V. Balakrishnan, *Linear Matrix Inequalities in System and Control Theory*. Society for Industrial and Applied Mathematics, 1994, vol. 15.

[18] I. Masubuchi, A. Ohara, and N. Suda, "Lmi-based output feedback controller design-using a convex parametrization of full-order controllers," in *Proceedings of 1995 American Control Conference - ACC'95*, vol. 5, 1995, pp. 3473–3477 vol.5.

[19] ——, "Lmi-based controller synthesis: A unified formulation and solution," *International Journal of Robust and Nonlinear Control*, vol. 8, pp. 669–686, 1998.

[20] R. J. Caverly and J. R. Forbes, "LMI properties and applications in systems, stability, and control theory," *CoRR*, vol. abs/1903.08599, 2019.